HIGH DETAIL STATIONARY OPTIMIZATION MODELS FOR GAS NETWORKS — PART 1: MODEL COMPONENTS.

MARTIN SCHMIDT, MARC C. STEINBACH, BERNHARD M. WILLERT

Abstract. Economic reasons and the regulation of gas markets create a growing need for mathematical optimization in natural gas networks. Real life planning tasks often lead to highly complex and extremely challenging optimization problems whose numerical treatment requires a breakdown into several simplified problems to be solved by carefully chosen hierarchies of models and algorithms. This paper presents stationary NLP type models of gas networks that are primarily designed to include fully nonlinear physics in the final optimization steps for mid term planning problems after fixing discrete decisions with coarsely approximated physics.

1. Introduction

Natural gas plays an increasingly important role as a source of primary energy. It is used for heating, in industrial processes, and even for generating electric power. The most economic means of transport over very long distances are tank ships for liquefied natural gas (LNG carriers), whereas pipelines are preferable for distances up to 4.000 km over land or 2.000 km offshore. One may distinguish three major types of gas pipeline networks:

- production networks (connecting gas fields with processing plants),
- transport networks (connecting processing plants with market areas),
- distribution networks (serving consumers in market areas).

Production networks are typically operated at low pressure and characterized by a linear or tree topology. Transport networks usually have a simple structure as well, but they are operated at high pressure. Distribution networks are again operated at lower pressure, but often they possess a very complex, closely meshed structure. Network operators are faced with various long, mid and short term planning problems. The focus of our modeling is primarily on mid term planning in transport and distribution networks: here the need and the potential for optimization are substantial due to highly volatile demands and market conditions, especially in a regulated environment like Europe.

Mathematical optimization in gas networks is very hard. Early approaches employ dynamic programming for fuel gas minimization in small linear or tree structured networks consisting of pipes and compressor stations [68, 69]; see [11] for a later survey. Here the physical models include a quadratic pressure loss along pipes ("Weymouth equation" [66, 31]), a maximum compression ratio for stations, and an idealized fuel consumption formula depending only on the compression ratio. In contrast, early models for transient simulation already include realistic gas dynamics and other network elements [65, 34, 33, 32, 73]. The authors of this work also propose extensions to steepest-descent optimization of stationary [29] and transient network operation [30, 63]. While the approaches above require fixed discrete decisions (compressor activity, valve settings, ...), later work proposes heuristics or nonlinear mixed-integer models (MINLP) for optimizing single compressor stations under prescribed pressure and flow conditions [46, 70, 10]. Aggregated models of compressor units in parallel operation are typical in this context, although some models of compressor power include simplified formulas of the adiabatic head. First studies with a focus on discrete aspects of these models are given in [12]. First attempts at using realistic operating ranges of individual compressor units in optimization can be found in [6, 72] where relaxation schemes are developed for the detailed model. (See [45] for a recent survey on modeling compressor machines).

Date: May 16, 2012.
2000 *Mathematics Subject Classification.* 90B10, 90C06, 90C30, 90C90.

More recent work, roughly since the last two decades, aims at addressing all network elements with both nonlinearities and discrete aspects. However, since full MINLP models of real networks are still intractable by current optimization algorithms (cf. [14]), two main branches of research have emerged. One branch employs piecewise linear approximations to obtain mixed-integer *linear* programs (MILP) [49, 56, 57, 15, 28, 41, 43, 42]. Based on such techniques, transient optimization by Simulated Annealing is addressed in [40, 44]. The second branch considers fully nonlinear physics models using fixed discrete decisions obtained from a coarser MILP solution. This yields NLP type approaches; see [71, 52, 62, 4, 5, 51] for stationary optimization, [17, 18, 60] for the transient case and [16] for a comparison of specific MILP and NLP approaches. Pressure loss models in the work above are still based on the Weymouth approximation, with the exception of [17, 18, 60] where discretizations of the Euler equations of gas dynamics are considered. The PDE are also considered in theoretical studies of controllability and stabilization of gas flow [27, 36, 26, 25, 3, 2, 7]. The theoretical analysis is currently restricted to very small passive networks.

Finally we would like to mention two aspects, gas temperature and composition (with mixing), that to the best of our knowledge are not included in any earlier optimization model—except for a mention of gas composition in [61]. The non-isothermal modeling presented below will cause additional nonlinearities in most component models and will add gas coolers and preheaters as new network elements.

Optimization algorithms for our purposes require a network model that covers a wide range of network states, and they benefit from adaptive accuracy control. Hence we develop *hierarchies* of component models that support various degrees of detail, in part up to the accuracy of simulation models. In contrast to earlier optimization models, we specifically consider

- a highly accurate flow model incorporating gas quality parameters, gas temperature, and uncontrolled mixing of different gas types;
- detailed compressor station models with various configurations rather than just single idealized compressors as replacements;
- complete models of turbo and piston compressor machines including their drives.

The current work is part of a joint effort with the German network operator Open Grid Europe and several accademic partners (project ForNe), where one of the goals is stationary network optimization incorporating fully nonlinear physics models, discontinuous mixed-integer aspects and stochastic data from demand profiles of customers [39]. Several publications are in preparation that report on further work in this context [23, 21, 55, 22].

The paper is organized as follows. In Sect. 2 we discuss general difficulties, goals and principles of gas network modeling for gradient-based optimization. Section 3 presents the individual model components in full detail, typically with several alternative formulations including smoothings or hierarchical simplifications. A model validation and special techniques for handling nonsmoothness along with optimization results for real gas networks of our industry partner will be provided in part 2 of this paper [54].

2. Model Structure

Gas networks consist primarily of pipelines transporting the gas from *entry nodes* (supply points) to *exit nodes* (discharge points). Several line segments may connect at entries and exits, or at *junction nodes* where no supply or demand occurs. The friction at inner pipe walls causes a pressure loss that must be compensated by *compressor stations* to produce the desired gas flow. Conversely, *control valve stations* reduce the pressure at the transition to low-pressure areas, and *(gate) valves* can interrupt the gas flow completely. Finally our model contains two types of fictitious elements: *short cuts* to connect nodes without impairing flow or pressure, and *resistors* to represent the pressure loss of apertures, station piping and further network elements like filters and measurement devices that are otherwise irrelevant for planning purposes. Note that *gas storage facilities* are not under control of the network operator in our context. Rather, they are owned by transport customers and are therefore modeled as entry or exit nodes, depending on the mode of operation.

Conserved	Phenomena / Effects	Network Element
Mass	Flow balance, mixing of gas types	Node
	Stationary flow	Pipe
Momentum	Velocity head, pressure gradient, gravity	Pipe
	Hydraulic pressure loss (friction)	Pipe, resistor
Energy	Heat exchange with ground, gravity	Pipe
	Joule–Thomson effect	All arcs except shortcut, valve
—	Interrelation of entry and exit pressures and temperatures, entry compressibility, flow, adiabatic head, power, efficiency and speed	Compressor
—	Interrelation of power, ambient temperature, speed and fuel or electricity consumption	Compressor drive

TABLE 1. Principal physical phenomena in gas networks.

Due to the size and complexity of real gas networks, a microscopic physics model capturing the 3d gas flow in pipes and technical devices would be impractical (even for simulation). We formulate a technical model over the network graph where spatial DAE describe 1d pipe flows and algebraic equations couple the head and tail quantities of other arcs as well as the inflow and outflow quantities at the nodes. Given a specific planning problem with some objective and certain restrictions, a suitable DAE discretization then yields a discrete-continuous optimization model involving integral and real node and arc variables restricted by possibly nonsmooth equality and inequality constraints. The most important physical phenomena and effects of our model are listed in Table 1. Substantial mathematical difficulties arise from the combination of complex physics with *discrete-continuous decisions* and *nonsmooth model components*. Consequently, our modeling will involve efforts toward reducing the degree of detail where possible and toward smoothing discontinuities so that derivative-based NLP solution techniques are applicable. The focus here is on NLP aspects; a discussion of the interplay with discrete aspects will be given in part 2 [54].

In summary, gas networks are complex technical systems consisting of various components associated with nodes and arcs of the network graph. Every component model must provide an adequate representation of its specific physical phenomena and technical processes subject to technical, contractual and legal constraints, where "adequateness" may depend on the purpose and required tolerance of numerical computations, the type of computations (simulation or optimization), and even the current accuracy within an iterative solution procedure.

For a better understanding of the model structure we categorize the components describing individual physical phenomena and technical behavior as follows:

physical laws: equations derived from a quantitative theory;
empirical laws: equations matching observations and experiments;
data fits: arbitrary equations fit to measured data by parameter estimation.

Typical examples include PDE systems of conservation laws for the dynamics of real gas (physical), formulae for hydraulic friction and compressibility (empirical), and the interrelation of power, speed, flow, etc. in compressor stations (data fits). All the data fits used below will be univariate or bivariate quadratic polynomials parameterized by a coefficient vector or matrix.

For numerical optimization algorithms based on first and second order derivatives we will often approximate model components to obtain C^2 functions in finite dimensions or to adjust the tradeoff between accuracy and effort. To this end we distinguish the following types of approximations in addition to the basic categories described above:

smoothings: C^2 approximations of less regular functions;
discretizations: grid approximations of differential equations;

Symbol	Explanation	Unit
q	Mass flow rate	$\mathrm{kg\,s^{-1}}$
Q	Volumetric flow rate ($q = \rho Q$)	$\mathrm{m^3\,s^{-1}}$
Q_0	Normal volumetric flow rate ($q = 3.6\rho_0 Q_0$)	$10^3\ \mathrm{m^3\,h^{-1}}$
P	Energy flow rate (heating power)	W
p	Pressure	Pa
T	Temperature	K
ρ	Density	$\mathrm{kg\,m^{-3}}$
v	Velocity	$\mathrm{m\,s^{-1}}$
m	Molar mass	$\mathrm{kg\,mol^{-1}}$
H_c	Calorific value (w.r.t. normal volume)	$\mathrm{J\,m^{-3}}$
ρ_0	Normal density	$\mathrm{kg\,m^{-3}}$
p_c	Pseudocritical pressure	Pa
T_c	Pseudocritical temperature	K
A, B, C	Coefficients of isobaric molar heat capacity	$\mathrm{J\,mol^{-1}\,K^{-\alpha}}$, $\alpha = 1, 2, 3$

TABLE 2. Main physical quantities in gas transport.

simplifications: arbitrary approximations of reduced effort and quality.

While simplifications are distinct model variants that may involve different sets of variables, smoothings and discretizations allow arbitrarily high precision by suitable choice of smoothing or grid parameters whose values control the tradeoff between approximation quality and numerical effort.

3. Model Hierarchy

In this section we present details of all components of our nonlinear optimization models for mid term planning problems in natural gas networks. For every model aspect we provide the most accurate formulation first, followed by simplified variants. Our focus lies on smooth C^2 formulations of the model constraints so that we will be able to solve the model with standard NLP solvers such as Ipopt [64], SNOPT [24] and the like. Discrete aspects will be mentioned where applicable, but will be assumed to be fixed in the current context.

3.1. Physical Quantities.

Gas flow in a network is described by the mass flow q and the state variables pressure p, density ρ, and temperature T. We also need the gas velocity v, volumetric flow Q, and a technical flow quantity that is common in the gas industry: normal volumetric flow Q_0. (Throughout the paper, subindex 0 refers to quantities at normal conditions, i.e., $T_0 = 273.15$ K and $p_0 = 101325$ Pa.)

Real gas is a mixture of several species. As usual, we do not model every species individually but rather use an emprirical model where a specific mixture is characterized by eight gas parameters: molar mass m, calorific value H_c, pseudocritical pressure p_c and temperature T_c, normal density ρ_0 and coefficients of the isobaric (constant-pressure) molar heat capacity, A, B, C. At exit nodes we finally need the heating power (energy flow) of the gas, $P = Q_0 H_c$.

Table 2 gives an overview of the main quantities and their physical units. Further physical and technical quantities will be introduced where they are needed. As we are considering stationary models, all quantities are constant in time.

3.2. Network Topology.

The network is modeled as a directed graph $G = (\mathbb{V}, \mathbb{A})$ whose node set (or vertex set) consists of entries $\mathbb{V}_+$, exits $\mathbb{V}_-$, and junctions $\mathbb{V}_0$,

$$\mathbb{V} = \mathbb{V}_+ \cup \mathbb{V}_- \cup \mathbb{V}_0, \tag{1}$$

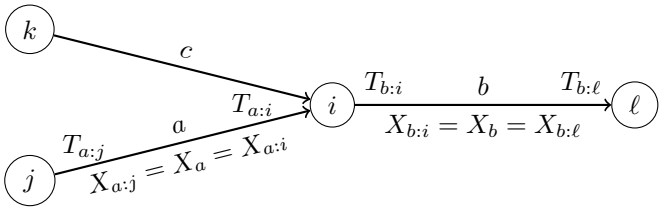

FIGURE 1. Notation for arc variables: gas quality parameters and temperature.

and whose arc set consists of pipes $\mathbb{A}_{\mathrm{pi}}$, resistors $\mathbb{A}_{\mathrm{re}}$, short cuts $\mathbb{A}_{\mathrm{sc}}$ (all passive), compressor stations $\mathbb{A}_{\mathrm{cs}}$, control valve stations $\mathbb{A}_{\mathrm{cv}}$ and valves $\mathbb{A}_{\mathrm{vl}}$ (all active),

$$\mathbb{A} = \mathbb{A}_{\mathrm{pi}} \cup \mathbb{A}_{\mathrm{re}} \cup \mathbb{A}_{\mathrm{sc}} \cup \mathbb{A}_{\mathrm{cs}} \cup \mathbb{A}_{\mathrm{cv}} \cup \mathbb{A}_{\mathrm{vl}}. \tag{2}$$

We denote nodes by $i, j \in \mathbb{V}$ and arcs by $a = ij \in \mathbb{A}$, using tail i and head j. The sets of ingoing and outgoing arcs at a node i are $\delta_i^- = \{a \in \mathbb{A} \colon a = ji\}$ and $\delta_i^+ = \{a \in \mathbb{A} \colon a = ij\}$, respectively; $\delta_i = \delta_i^- \cup \delta_i^+$ denotes all arcs incident on i.

The principal node and arc variables are pressures p_i and mass flows q_a. Arc quantities may have different values at tail and head, such as $p_{a:i}$ and $p_{a:j}$, or may be constant, like $q_a = q_{a:i} = q_{a:j}$. Pipe quantities may in general depend on the spatial coordinate $x \in [0, L_a]$ where, e.g., $p_{a:i} = p_a(0)$ and $p_{a:j} = p_a(L_a)$. Except for pressure, all arc quantities may be discontinuous across nodes. For instance, we define a vector X of gas parameters (cf. Sect. 3.1) and an extended vector $\bar{X}$,

$$X := (m, H_c, p_c, T_c, \rho_0, A, B, C), \qquad \bar{X} := (X, T). \tag{3}$$

All components of $\bar{X}$ satisfy identical mixing equations that yield jumps at the mixing node. However, X is constant on every arc $a = ij$ whereas $T_{a:i}, T_{a:j}$ may differ, as illustrated in Fig. 1.

Most arcs admit flow in both directions: positive from i to j or negative from j to i. The mass flow vector $q_{\mathbb{A}} := (q_a)_{a \in \mathbb{A}}$ thus defines respective *state-dependent* sets of inflow and outflow arcs at node i,

$$\mathcal{I}_i(q_{\mathbb{A}}) := \{a \in \delta_i^- \colon q_a \geq 0\} \cup \{a \in \delta_i^+ \colon q_a \leq 0\}, \tag{4}$$

$$\mathcal{O}_i(q_{\mathbb{A}}) := \{a \in \delta_i^- \colon q_a < 0\} \cup \{a \in \delta_i^+ \colon q_a > 0\}. \tag{5}$$

Several component models depend on inflow and outflow quantities of an arc, such as

$$p_{a,\mathrm{in}}(q_a) = \begin{cases} p_{a:i}, & q_a \geq 0, \\ p_{a:j}, & q_a < 0, \end{cases} \qquad p_{a,\mathrm{out}}(q_a) = \begin{cases} p_{a:j}, & q_a \geq 0, \\ p_{a:i}, & q_a < 0, \end{cases} \tag{6}$$

hence these models become *nonsmooth* at $q_a = 0$. In the following we will usually omit the flow argument, writing $p_{a,\mathrm{in}}$ or $\mathcal{O}_i$ for brevity.

3.3. **Nodes.** Every node $i \in \mathbb{V}$ has an associated geodesic height h_i, a pressure variable p_i with technical or contractual bounds, $p_i \in [p_i^-, p_i^+]$, and an extended gas parameter variable $\bar{X}_i$. Conservation of mass yields the flow balance equation

$$q_i^{\mathrm{ext}} + \sum_{a \in \delta_i^-} q_a - \sum_{a \in \delta_i^+} q_a - \sum_{a \in \delta_i^{\mathrm{cs}}} q_a^{\mathrm{fuel}} = 0. \tag{7}$$

Here q_i^{ext} is the externally supplied or discharged gas at node i and δ_i^{cs} is the set of compressor stations that take their fuel gas q_a^{fuel} from node i. The flows q_i^{ext} are determined by contracts with providers and consumers, where $q_i^{\mathrm{ext}} \geq 0$ at entries, $q_i^{\mathrm{ext}} \leq 0$ at exits and $q_i^{\mathrm{ext}} = 0$ at junctions. In addition, entry and exit contracts include bounds on the energy flow,

$$P_i \in [P_i^-, P_i^+], \quad i \in \mathbb{V}_+ \cup \mathbb{V}_-, \tag{8}$$

where $P_i^- = P_i^+$ results in P_i being fixed. These bounds induce implicit constraints on the discharged mass flow q_i^{ext} and on the calorific value $H_{c,i}$.

Gas flows entering node i are assumed to mix perfectly. The vector of outflow composition and temperature, $\bar{X}_i$, is obtained as convex combination with weights given by the distribution of absolute molar inflows,

$$\bar{X}_i = \frac{\hat{q}_i^{\mathrm{ext}} \bar{X}_i^{\mathrm{ext}} + \sum_{a \in \mathcal{I}_i} \hat{q}_a \bar{X}_{a:i}}{\hat{q}_i^{\mathrm{ext}} + \sum_{a \in \mathcal{I}_i} \hat{q}_a}, \quad \hat{q}_a := \frac{|q_a|}{m_a}, \quad \bar{X}_{a:i} = \bar{X}_i \; \forall a \in \mathcal{O}_i. \tag{9}$$

If i is an entry, we have $\hat{q}_i^{\mathrm{ext}} := q_i^{\mathrm{ext}}/m_i \geq 0$ and inflow parameters $\bar{X}_i^{\mathrm{ext}}$ are given externally. Otherwise we set $\hat{q}_i^{\mathrm{ext}} := 0$ so that the associated terms vanish in (9). If i is an exit, the outflow parameters are obtained as $\bar{X}_i^{\mathrm{ext}} = \bar{X}_i$. Note that the mixing equations are nonsmooth since $\mathcal{I}_i(q_{\mathbb{A}})$ and $\mathcal{O}_i(q_{\mathbb{A}})$ are state-dependent: first partial derivatives of $\bar{X}_i$ with respect to q_a will generally be discontinuous at $q_a = 0$. There is no suitable (multivariate!) smoothing for (9) yet: we could offer an MPEC reformulation with complementarity constraints, but it would significantly enlarge the model, and in our experience it is not helpful in an NLP context. Therefore we either assume that gas quality parameters and temperature are fixed throughout the network (thus simplifying the overall model considerably), or we assume that all flow *directions* are fixed so that $\mathcal{I}_i$ and $\mathcal{O}_i$ are independent of $q_{\mathbb{A}}$; see [54] for a detailed discussion.

Note finally that stationary network operation requires as a necessary condition that external flows and the fuel consumption of compressors are globally balanced:

$$\sum_{i \in \mathbb{V}_+ \cup \mathbb{V}_-} q_i^{\mathrm{ext}} - \sum_{a \in \mathbb{A}_{\mathrm{cs}}} q_a^{\mathrm{fuel}} = 0. \tag{10}$$

3.4. **Arcs.** Every arc $a = ij \in \mathbb{A}$ has an associated mass flow variable q_a with technical or contractual bounds, $q_a \in [q_a^-, q_a^+]$, a gas parameter variable X_a, and two temperature variables $T_{a:i}, T_{a:j}$.

3.4.1. *Valves.* Valves are purely combinatorial in nature, with the two states *open* and *closed*. Open valves do not impair pressure or temperature, i.e., $p_i = p_j$ and $T_{a:i} = T_{a:j}$. Closed valves act like absent arcs, having zero flow and decoupled pressures p_i, p_j and temperatures $T_{a:i}, T_{a:j}$.

3.4.2. *Short Cuts.* Short cuts are fictitious elements acting like open valves. They are mainly used for modeling special situations, such as fictitious entry or exit flows at joint venture pipes, or the supply of different gas mixtures at a single entry node.

3.4.3. *Resistors.* Resistors are again fictitious elements. They model the summarized resistance of apertures, station piping, filters etc., which cause a pressure loss in the direction of flow. Depending on the available data, the absolute pressure loss is either assumed to be constant,

$$p_i - p_j = \mathrm{sign}(q_a)\xi_a, \tag{11}$$

or a quadratic function of the flow (Darcy–Weisbach model, with a fictitious diameter D_a),

$$p_i - p_j = \frac{1}{2}\zeta_a \rho_{a,\mathrm{in}} |v_{a,\mathrm{in}}| v_{a,\mathrm{in}} = \frac{8\zeta_a}{\pi^2 D_a^4} \frac{|q_a| q_a}{\rho_{a,\mathrm{in}}}. \tag{12}$$

Here $\rho_{a,\mathrm{in}}, v_{a,\mathrm{in}}$ refer to the inflow side of arc a, and ξ_a, ζ_a are resistance coefficients of the element. The pressure loss is accompanied by a temperature drop due to the Joule–Thomson effect (99). Clearly, (11) and (12) have discontinuities of respective orders zero and one at $q_a = 0$. For the absolute value function in (12) we employ the standard smoothing approximation

$$|x| \approx \sqrt{x^2 + \epsilon} \tag{13}$$

with a suitable smoothing parameter $\epsilon > 0$. Based on (13) we also obtain standard smoothings for $\min(x, y)$, $\max(x, y)$ and $\mathrm{sign}(x)$ (see Fig. 2), all of which are used here or later on:

$$\min(x, y) = y - \frac{1}{2}(|d| - d) \approx y - \frac{1}{2}\left(\sqrt{d^2 + \epsilon} - d\right), \quad d := x - y, \tag{14}$$

$$\max(x, y) = y + \frac{1}{2}(|d| + d) \approx y - \frac{1}{2}\left(\sqrt{d^2 + \epsilon} + d\right), \quad d := x - y, \tag{15}$$

$$\mathrm{sign}(x) = \frac{x}{|x|} \approx \frac{x}{\sqrt{x^2 + \epsilon}}. \tag{16}$$

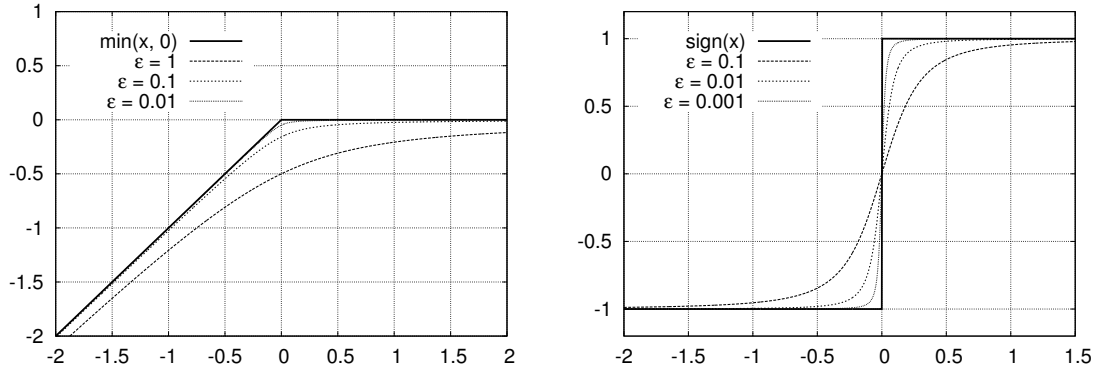

FIGURE 2. Smoothing of $\max(x, 0)$ and $\operatorname{sign}(x)$ with several values of ϵ.

All these approximations except (16) converge uniformly to the exact function as $\epsilon \to 0$.

3.4.4. *Pipes.* Gas networks consist primarily of *pipeline segments:* sequences of cylindrically shaped pipes that are welded together. Basic parameters of a pipe $a = ij \in \mathbb{A}_{\mathrm{pi}}$ are its length L_a, diameter D_a, and roughness of the inner wall k_a, yielding the cross-sectional area $A_a = \frac{\pi}{4} D_a^2$ and the slope $s_a = (h_j - h_i)/L_a \in [-1, +1]$. Our model also needs the heat transfer coefficient $c_{\mathrm{HT},a}$ and temperature of the surrounding soil $T_{\mathrm{soil},a}$. Pipeline segments consisting of pipes with identical or nearly identical parameters (except length) are usually modeled as single pipe arcs.

State variables are averaged over the cross-section and depend only on the position $x \in [0, L_a]$. In addition to the mass flow $q_a(x)$ and the pressure $p_a(x)$ we consider the gas density $\rho_a(x)$, temperature $T_a(x)$ and velocity $v_a(x)$. The latter two are subject to technical or legal bounds, $T_a(x) \in [T_a^-, T_a^+]$ and $|v_a(x)| \le v_a^+$. Typical values in our planning problems are $T_a^- = T_0$ (0 °C), $T_a^+ = T_0 + 45\,\mathrm{K}$ (45 °C), and $v_a^+ = 20\,\mathrm{m\,s^{-1}}$. In the remainder of this section we drop the index a.

Instationary gas dynamics in a pipe are governed by a *hyperbolic system of PDE*, the non-isothermal Euler equations for compressible fluids (see, e.g., [19, 38]):

$$\frac{\partial \rho}{\partial t} + \frac{\partial (\rho v)}{\partial x} = 0, \tag{17}$$

$$\frac{\partial (\rho v)}{\partial t} + \frac{\partial p}{\partial x} + \frac{\partial (\rho v^2)}{\partial x} + g\rho \frac{\partial h}{\partial x} + \lambda(q) \frac{|v| v}{2D} \rho = 0, \tag{18}$$

$$A\rho c_p \left(\frac{\partial T}{\partial t} + v \frac{\partial T}{\partial x} \right) - A \left(1 + \frac{T}{z} \frac{\partial z}{\partial T} \right) \frac{\partial p}{\partial t} - A v \frac{T}{z} \frac{\partial z}{\partial T} \frac{\partial p}{\partial x} + A\rho v g \frac{\partial h}{\partial x} + \pi D c_{\mathrm{HT}} (T - T_{\mathrm{soil}}) = 0. \tag{19}$$

These equations describe the conservation of mass, momentum and energy, respectively. (For the physical details we refer to the literature.) We assume constant slope, $\partial h/\partial x \equiv s$, and replace velocity by mass flow as the primary flow variable, $q = A\rho v$. As we are considering the stationary case only, all time derivatives vanish. The *continuity equation* (17) thus yields constant mass flow $q(x) \equiv q$,

$$\frac{\partial q}{\partial x} = 0, \tag{20}$$

and the *momentum* and *energy equations* (18), (19) reduce to a semi-implicit *system of ODE* for pressure and temperature,

$$\frac{\partial p}{\partial x} + \frac{q^2}{A^2} \frac{\partial}{\partial x} \frac{1}{\rho} + g\rho s + \lambda(q) \frac{|q| q}{2A^2 D \rho} = 0, \tag{21}$$

$$q c_p \frac{\partial T}{\partial x} - \frac{qT}{\rho z} \frac{\partial z}{\partial T} \frac{\partial p}{\partial x} + qgs + \pi D c_{\mathrm{HT}} (T - T_{\mathrm{soil}}) = 0. \tag{22}$$

Symbol	Explanation	Unit
L	Length	m
D	Diameter	m
k	Roughness of inner wall	m
A	Cross-sectional area	m^2
c_{HT}	Heat transfer coefficient	$\mathrm{J\,m^{-2}\,K^{-1}\,s^{-1}}$
T_{soil}	Soil temperature	K
λ	Friction coefficient	1
Re	Reynolds number	1
z	Compressibility factor	1
ν	Kinematic viscosity	$\mathrm{m^2\,s^{-1}}$
η	Dynamic viscosity ($\eta = \nu\rho$)	$\mathrm{kg\,m^{-1}\,s^{-1}}$
V	Molar gas volume	$\mathrm{m^3\,mol^{-1}}$
c_p	Specific isobaric heat capacity	$\mathrm{J\,kg^{-1}\,K^{-1}}$

TABLE 3. Technical and physical quantities associated with pipes.

This ODE system is coupled with an equation of state for real gas to express the density in terms of pressure and temperature. As equation of state we consider the thermodynamical standard equation here,

$$\rho = \gamma_0 \frac{p}{z(p,T)T} \quad \text{with} \quad \gamma_0 = \frac{\rho_0 z_0 T_0}{p_0}. \tag{23}$$

The gas dynamics model (20)–(23) is physically exact, except that only empirical models exist for the friction coefficient $\lambda(q)$ and the compressibility factor $z(p,T)$, and that exact data for the heat exchange with the surrounding soil are unavailable in practice.

A commonly used alternative to the thermodynamical standard equation is the empirical equation of Redlich–Kwong [50],

$$p = \frac{RT}{V-b} - \frac{a}{\sqrt{T}\,V(V+b)} \quad \text{with} \quad V = \frac{m}{\rho}. \tag{24}$$

Here the parameters are $a = \Omega_a R^2 T_c^{2.5}/p_c$, $b = \Omega_b R T_c/p_c$, $\Omega_a = (9(2^{1/3}-1))^{-1}$, $\Omega_b = 2^{1/3} - 1/3$, where R is the universal gas constant and V the molar gas volume ($\mathrm{m^3\,mol^{-1}}$). According to Wikipedia [67], (24) is appropriate for gas states satisfying $p_r < T_r/2$, where p_r and T_r denote relative pressure and temperature, respectively,

$$p_r = \frac{p}{p_c}, \qquad T_r = \frac{T}{T_c}. \tag{25}$$

The standard equation (23) involves the compressibility factor z which describes the deviation of real gas from ideal gas. Two empirical models are commonly used in practice: the formula of the American Gas Association (AGA) [37, 57],

$$z(p,T) = 1 + 0.257 p_r - 0.533 \frac{p_r}{T_r}, \tag{26}$$

and the formula of Papay ([48], see also [37, 57] or [53, Chap. 2]),

$$z(p,T) = 1 - 3.52 p_r \exp(-2.26 T_r) + 0.274 p_r^2 \exp(-1.878 T_r). \tag{27}$$

The AGA formula is appropriate for pressures up to 70 bar while (27) is appropriate up to 150 bar (see Fig. 3). There exist models with much wider ranges of validity, such as the ISO standard model AGA8-DC92 [59] and the GERG-2004 model [35]. These are highly complicated and unnecessarily accurate in our optimization context, however, and therefore not considered here.

The friction coefficient $\lambda(q)$ in (21) has a piecewise definition: we need to distinguish *laminar* flow ($|q|$ small) and *turbulent* flow ($|q|$ large) as determined by a certain critical value of the

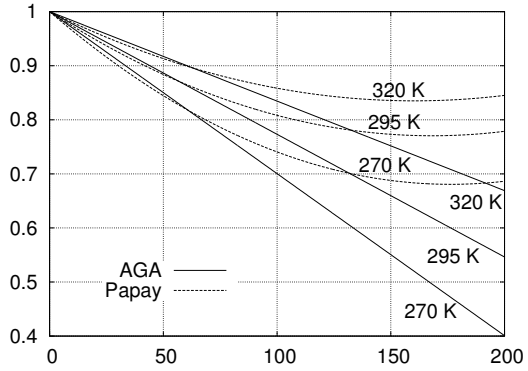

FIGURE 3. Compressibility factor z vs. pressure (bar): empirical models.

Reynolds number [38, 53]:

$$\mathrm{Re}(q) = \frac{D}{A\eta}|q| = \frac{D}{\eta}\rho|v| = \frac{D}{\nu}|v|, \quad \mathrm{Re}_{\mathrm{crit}} \approx 2320. \tag{28}$$

(Here ν and η denote the kinematic and dynamic viscosity of the gas, respectively.) For $0 \le \mathrm{Re} \le \mathrm{Re}_{\mathrm{crit}}$ the flow is laminar and the friction coefficient is given exactly by the law of Hagen–Poiseuille [20]

$$\lambda^{\mathrm{HP}}(q) = \frac{64}{\mathrm{Re}(q)}. \tag{29}$$

For $\mathrm{Re} > \mathrm{Re}_{\mathrm{crit}}$ the flow is turbulent. In this case the friction coefficient depends on the pipe diameter and the roughness of its inner wall, but no exact formula exists. Among various empirical models (like Gazprom, Hofer, Nikuradze [37] and Hazen–Williams [8]), the implicit equation of Prandtl–Colebrook is generally considered most accurate [53, Chap. 9],

$$\frac{1}{\sqrt{\lambda^{\mathrm{PC}}(q)}} = -2\log_{10}\left(\frac{2.51}{\mathrm{Re}(q)\sqrt{\lambda^{\mathrm{PC}}(q)}} + \frac{k}{3.71D}\right). \tag{30}$$

We denote the combination of (29) and (30) by $\lambda^{\text{HP-PC}}$ and extend it to negative flows by setting $\lambda^{\text{HP-PC}}(-|q|) = -\lambda^{\text{HP-PC}}(|q|)$. The resulting flow-dependent part of the friction term in the momentum equation (21) then reads

$$\frac{\lambda^{\text{HP-PC}}(q)}{2A^2D}|q|q. \tag{31}$$

This HP-PC friction term (see Fig. 4) has jump discontinuities caused by $\lambda^{\text{HP-PC}}$ at the transition points between laminar and turbulent flow, $\mathrm{Re}(\pm q) = \mathrm{Re}_{\mathrm{crit}}$, and the second order derivative has a jump discontinuity at $q = 0$ caused by $|q|q$. To avoid discontinuities, we replace the HP-PC friction term by a global smooth approximation ϕ in our model (which has originally been developed for optimization in drinking water networks [8, 9]):

$$\phi(q) = r\left(\sqrt{q^2 + a^2} + b + \frac{c}{\sqrt{q^2 + d^2}}\right)q, \quad a, d > 0. \tag{32}$$

For $|q| \to \infty$ this provides an asymptotically correct second order approximation of the HP-PC friction term if the parameters r, b, c satisfy the following relations:

$$r = \frac{\tilde{\lambda}}{2A^2D}, \quad \tilde{\lambda} = (2\log_{10}\beta)^{-2}, \quad b = 2\delta, \quad c = (\ln\beta + 1)\delta^2 - \frac{a^2}{2}, \tag{33}$$

where

$$\alpha = \frac{2.51A\eta}{D}, \quad \beta = \frac{k}{3.71D}, \quad \delta = \frac{2\alpha}{\beta\ln 10}. \tag{34}$$

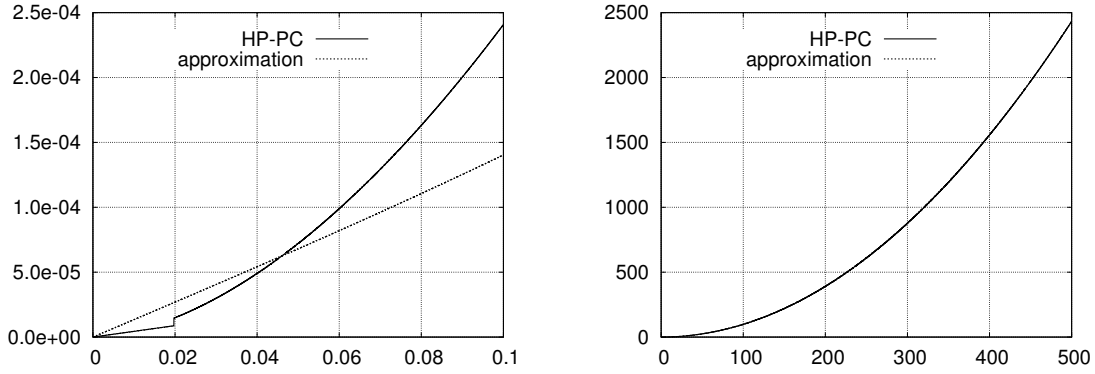

FIGURE 4. HP-PC friction term vs. mass flow ($\mathrm{kg\,s^{-1}}$) and smooth approximation: transition from laminar to turbulent flow (left) and highly turbulent flow (right).

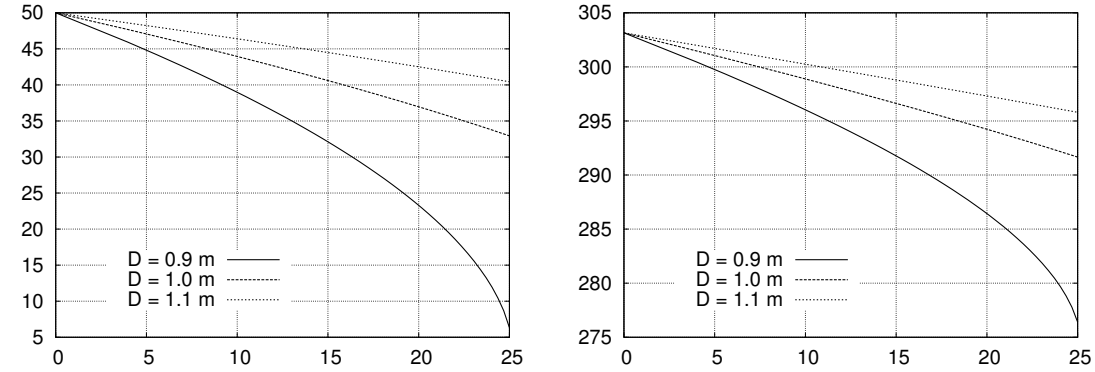

FIGURE 5. Profiles of pressure (bar, left) and temperature (K, right) along three horizontal pipes ($L = 25$ km, $D = 1.0 \pm 0.1$ m, $k = 0.06$ mm; $q = 500\ \mathrm{kg\,s^{-1}}$).

The choice of smoothing parameters a and d is up to the modeler; together they determine the slope ϕ' at $q = 0$ and the relative contributions of the two square root terms for small flow values.

Finally we consider the specific isobaric heat capacity c_p of real gas, which is the amount of energy required to raise the temperature of one kilogram of gas by one Kelvin at constant pressure. Here we use the model given in [37],

$$c_p(p,T) = \frac{1}{m}\left(\tilde{c}_p^0(T) + \Delta\tilde{c}_p(p,T)\right), \tag{35}$$

where $\tilde{c}_p^0$ is the molar heat capacity of ideal gas ($\mathrm{J\,mol^{-1}\,K^{-1}}$) and $\Delta\tilde{c}_p$ is a correction for real gas. The ideal gas term $\tilde{c}_p^0$ is modeled as a quadratic data fit [37],

$$\tilde{c}_p^0(T) = A + BT + CT^2, \tag{36}$$

where A, B, C depend on the specific gas mixture, cf. (3). The real gas correction is given by

$$\Delta\tilde{c}_p(p,T) = -R\int_0^p \frac{1}{p}\left(2T\frac{\partial z}{\partial T} + T^2\frac{\partial^2 z}{\partial T^2}\right)\mathrm{d}p. \tag{37}$$

This integral evaluates to zero if z is modeled by the AGA formula (26).

The spatial ODE model of stationary gas dynamics in pipes is now complete. Typical pressure and temperature profiles along a pipe, i.e., solutions $p(x)$ and $T(x)$ of (21) and (22), are illustrated in Fig. 5.

3.4.5. *Pipe Models.* There are several possibilities for representing the above ODE system as equality constraints of the general form

$$c_a^{\text{momentum}}(p_i, p_j, q_a) = 0, \tag{38}$$

$$c_a^{\text{energy}}(p_i, p_j, T_{a:i}, T_{a:j}, q_a) = 0. \tag{39}$$

Ideally we would like to characterize *exact* solutions of (21) and (22) in this form. Although this is impossible in full generality, exact integrals to the momentum equation (21) can be derived in the isothermal case under certain assumptions. These exact integrals from the Diploma thesis [47] will be presented in Sect. 3.4.6. Alternatively one may use a direct discretization of the ODE system, which we sketch for a simple backward Euler scheme in Sect. 3.4.7. Finally there exist commonly used isothermal approximations to the momentum equation in the engineering literature. We derive a similar approximation for the energy equation in Sect. 3.4.8.

3.4.6. *Exact Solutions.* Under the key assumption of isothermal flow ($T(x) \equiv \text{const}$) we can derive the desired implicit representation (38) of solutions to the momentum equation in three cases [47]:

(1) for horizontal pipes with the Papay compressibility model;
(2) for horizontal pipes with the AGA compressibility model;
(3) for inclined pipes with the AGA compressibility model.

We consider a fixed temperature T, write $z(p)$ for $z(p, T)$, and recall that $T_r = T/T_c$. In case (1) the horizontal pipe has slope $h'(x) \equiv 0$, and we obtain:

$$0 = \phi(q)L + q^2 \ln \frac{p_i z(p_j)}{p_j z(p_i)} + \frac{\gamma_0}{\beta T}\left(\frac{1}{2}\ln\frac{z(p_j)}{z(p_i)} + \frac{\alpha}{\omega}\delta(p_i, p_j)\right). \tag{40}$$

Here α, β, γ_0 are constants from the Papay model (27) and from the equation of state (23),

$$\alpha = \frac{3.52}{p_c}\exp(-2.26T_r), \quad \beta = \frac{0.274}{p_c^2}\exp(-1.878T_r), \quad \gamma_0 = \frac{\rho_0 z_0 T_0}{p_0}, \tag{41}$$

and δ, ω are defined as follows (where $4\beta - \alpha^2 > 0$ if $T \geq 0.94T_c \approx 180$ K):

$$\delta(p_i, p_j) = \arctan\frac{z'(p_j)}{\omega} - \arctan\frac{z'(p_i)}{\omega}, \quad \omega = \sqrt{4\beta - \alpha^2}. \tag{42}$$

In case (2) the resulting formula is slightly simpler:

$$0 = \phi(q)L + q^2 \ln \frac{p_i z(p_j)}{p_j z(p_i)} + \frac{\gamma_0}{\alpha T}\left(\frac{1}{\alpha}\ln\frac{z(p_i)}{z(p_j)} + p_j - p_i\right). \tag{43}$$

Here γ_0 is the above constant and α is a constant obtained from the AGA model (26),

$$\alpha = \frac{0.257}{p_c} - \frac{0.533}{p_c T_r}. \tag{44}$$

In case (3) the inclined pipe has constant slope $h'(x) \equiv s$, and with α from (44) we define

$$\sigma(q) = \frac{gs\gamma_0^2}{\alpha^2 T^2 \phi(q)}. \tag{45}$$

We have to distinguish two cases: $\sigma(q) = -1$ and $\sigma(q) \neq -1$. For $\sigma = -1$ it can be shown that p_i, p_j, q satisfy

$$0 = \phi(q)L - q^2\left(\ln\frac{p_j}{p_i} - \frac{1}{2}\ln\frac{1+2\alpha p_j}{1+2\alpha p_i}\right) + \frac{\gamma_0}{4\alpha T}\left(p_j z(p_j) - p_i z(p_i) - \frac{1}{2\alpha}\ln\frac{1+2\alpha p_j}{1+2\alpha p_i}\right). \tag{46}$$

The case $\sigma \neq -1$ is considerably more complicated: now the solution is given by

$$0 = L - \frac{q^2}{\phi(q)}\left(\ln\frac{p_j}{p_i} - \zeta\right) + \frac{\sigma}{\sigma+1}\frac{T}{gs\gamma_0}\left(\alpha(p_j - p_i) + \frac{\sigma}{\sigma+1}(\zeta - 2I(\nu_i, \nu_j)) - \frac{1}{\sigma+1}\zeta\right), \tag{47}$$

where $\nu = 1 + \alpha p$ and

$$\zeta = \frac{1}{2}\ln\left|\frac{z(p_j)^2 + (\alpha p_j)^2\sigma}{z(p_i)^2 + (\alpha p_i)^2\sigma}\right|, \qquad I(r, s) = \int_r^s \frac{\mathrm{d}\nu}{(\sigma+1)\nu^2 - 2\sigma\nu + \sigma}. \tag{48}$$

The integral $I(r,s)$ has an analytic solution which we omit here for simplicity. As the formulae for $\sigma \neq -1$ are highly complicated and involve an absolute value in computing ζ, they do not appear well suited for optimization.

3.4.7. *ODE Discretization.* Next we consider a discretization of the ODE system on a spatial grid $\Delta = \{x_k\}_{k=0}^d$ with $0 = x_0 < \cdots < x_d = L$. Denote the subinterval length by $\Delta x_k = x_k - x_{k-1}$, $k = 1, \ldots, d$, and let

$$p_k = p(x_k), \quad T_k = T(x_k), \quad \rho_k = \rho(x_k), \quad z_k = z(p_k, T_k), \quad k = 0, \ldots, d. \tag{49}$$

Here

$$p_0 = p_i, \quad p_d = p_j, \quad T_0 = T_{a:i}, \quad T_d = T_{a:j}, \quad \rho_0 = \rho_{a:i}, \quad \rho_d = \rho_{a:j}. \tag{50}$$

This yields backward differences

$$p'(x_k) \approx \frac{p_k - p_{k-1}}{\Delta x_k} = \frac{\Delta p_k}{\Delta x_k}, \quad T'(x_k) \approx \frac{T_k - T_{k-1}}{\Delta x_k} = \frac{\Delta T_k}{\Delta x_k}, \quad \rho'(x_k) \approx \frac{\rho_k - \rho_{k-1}}{\Delta x_k} = \frac{\Delta \rho_k}{\Delta x_k}. \tag{51}$$

Using the pipe slope $s = (h_j - h_i)/L$, the partial derivative $z_{T,k} = \partial_T z(p_k, T_k)$, and considering a backward Euler scheme for the ODE we obtain the discretization of (21) and (22):

$$\rho_k \frac{\Delta p_k}{\Delta x_k} - \frac{q^2}{A^2} \frac{\Delta \rho_k}{\Delta x_k} \frac{1}{\rho_k} + gs\rho_k^2 + \phi(q) = 0, \quad k = 1, \ldots, d, \tag{52}$$

$$\left(c_{p,k} \frac{\Delta T_k}{\Delta x_k} - \frac{T_k z_{T,k}}{\rho_k z_k} \frac{\Delta p_k}{\Delta x_k} + gs \right) q + \pi D c_{\mathrm{HT}} (T_k - T_{\mathrm{soil}}) = 0, \quad k = 1, \ldots, d. \tag{53}$$

To complete the pipe flow model, the equation of state (23) or (24) and the specific heat capacity (35)–(37) are evaluated at the corresponding grid points x_k. Note that one obtains an implicit discretization (as desired) if the flow is positive but an explicit scheme otherwise. Further considerations are therefore in order if the flow directions are not fixed. Of course, one may also choose suitable higher order discretizations.

3.4.8. *ODE Approximation.* Most of the literature on simulation and optimization in gas networks does not address the full system of Euler equations but considers an isothermal approximation where the energy equation is dropped, as in Sect. 3.4.6. With certain mean values p_m, T_m of pressure and temperature along the pipe, the momentum equation then yields a commonly used quadratic relation between flow and initial and final pressures [1, 38],

$$p_j^2 - \left(p_i^2 - \Lambda(q) q |q| \frac{e^S - 1}{S} \right) e^{-S} = 0 \tag{54}$$

where

$$\Lambda(q) = \frac{L}{A^2 D} \frac{z_m T_m}{\gamma_0} \lambda(q), \quad S = 2Lgs \frac{\gamma_0}{z_m T_m}, \quad z_m = z(p_m, T_m). \tag{55}$$

Here $T_m = \frac{1}{2}(T_{a:i} + T_{a:j})$ or simply $T_m = \frac{1}{2}(T_a^- + T_a^+)$, and p_m is approximated by [53, Chap. 9]

$$p_m = \frac{2}{3} \left(p_i + p_j - \frac{p_i p_j}{p_i + p_j} \right) \tag{56}$$

or by the state-independent value

$$p_m = \frac{1}{2} \left(\max(p_i^-, p_j^-) + \min(p_i^+, p_j^+) \right). \tag{57}$$

To achieve smoothness in (54) we replace the HP-PC friction term again by our approximation ϕ, leading to a slightly modified definition of $\Lambda(q)$. Note finally that s and S vanish in case of a horizontal pipe, which yields the simplification

$$p_i^2 - p_j^2 = \Lambda(q) q |q|. \tag{58}$$

Further quadratic approximations of the pipe pressure loss, such as the Weymouth equation or the "Panhandle B" equation, can be found in [53].

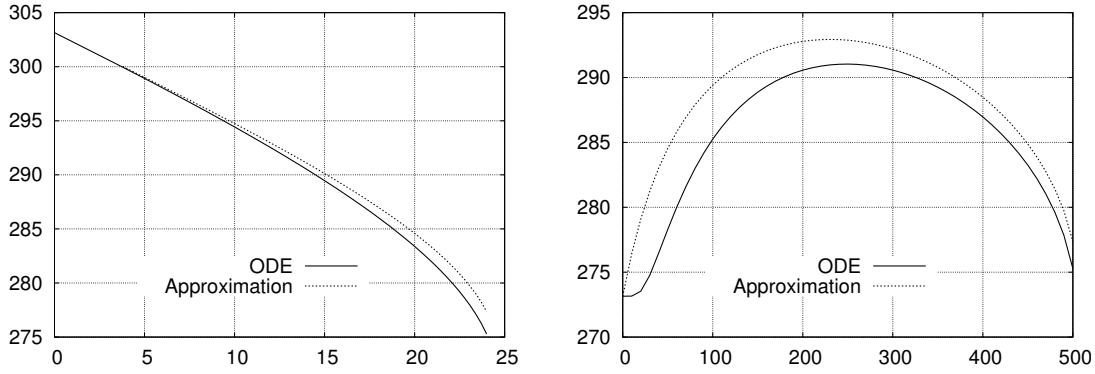

FIGURE 6. Temperature profile of a pipe (left; $L = 24$ km, $D = 1$ m, $k = 0.1$ mm, $q = 500\ \mathrm{kg\,s^{-1}}$) and outflow temperature vs. mass flow (right).

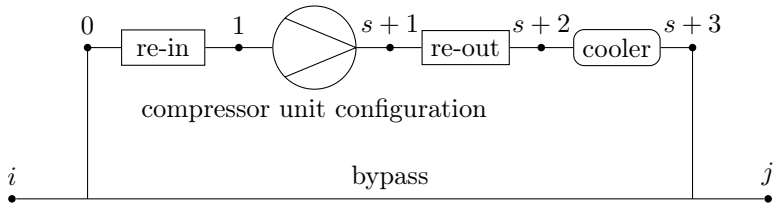

FIGURE 7. Compressor station (schematic overview).

Following the main ideas of these derivations we obtain a similar approximation of the energy equation (22). Let $z_m = z(p_m, T_m)$, $z_{T,m} = \partial_T z(p_m, T_m)$ and replace ρ by $\rho_m = \gamma_0 p_m/(z_m T_m)$. Then a single Euler step on $[0, L]$ yields

$$q(T_{\mathrm{out}} - T_{\mathrm{in}} + \gamma_1) - \gamma_2 T_{\mathrm{out}} q(p_j - p_i) + \gamma_3(T_{\mathrm{out}} - T_{\mathrm{soil}}) = 0 \tag{59}$$

where

$$\gamma_1 = \frac{gsL}{c_p}, \quad \gamma_2 = \frac{z_{T,m}}{c_p \rho_m z_m}, \quad \gamma_3 = \frac{\pi D c_{\mathrm{HT}} L}{c_p}. \tag{60}$$

For horizontal pipes, γ_1 vanishes and the approximation simplifies to

$$q(T_{\mathrm{out}} - T_{\mathrm{in}}) - \gamma_2 T_{\mathrm{out}} q(p_j - p_i) + \gamma_3(T_{\mathrm{out}} - T_{\mathrm{soil}}) = 0. \tag{61}$$

Clearly, (59) and (61) capture the two main effects of the energy equation: changes of the gas temperature caused by pressure changes and exchange of thermal energy with the soil; see Fig. 6.

3.4.9. *Compressor Stations.* A compressor station $a = ij \in \mathbb{A}_{\mathrm{cs}}$ can be operated in three modes: closed, bypass, or active. A *closed* station blocks the gas flow completely, hence inflow and outflow pressures and temperatures p_i, p_j and $T_{a:i}, T_{a:j}$ are decoupled. In *bypass mode* the gas passes the station uncompressed, leading to identical inflow and outflow pressures and temperatures, $p_i = p_j$ and $T_{a:i} = T_{a:j}$. The direction of flow through a station may reverse in bypass mode. In *active mode* the gas flows through some combination of compressor units that increase the pressure. Since this raises the gas temperature as well, the station has a gas cooler that will be activated at a certain threshold. The combined resistance of apertures, station piping and filters are modeled as in- and outgoing resistors. Figure 7 gives a schematic overview of a compressor station.

The remainder of this section concentrates on the active mode wherein the compressor units located in the station can be combined in various *configurations*: units may operate in parallel (to obtain high throughput) and parallel combinations may be connected in series (to obtain a high compression ratio). Every configuration is such a series of parallel stages that can be represented as a subgraph replacing the arc from 1 to $s + 1$ in Fig. 7. For instance, Fig. 8 illustrates the set of all possible configurations with two machines.

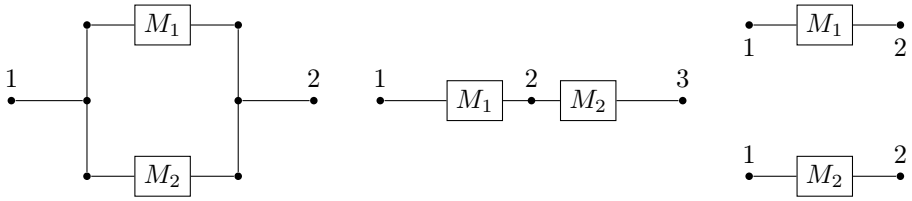

FIGURE 8. Configurations of a compressor station with two machines.

Symbol	Explanation	Unit
$a(l,k)$	Compressor unit k at stage l	—
$i(l,k)$	Inflow node of unit k at stage l	—
$j(l,k)$	Outflow node of unit k at stage l	—
$p_{a,l}$	Inflow pressure at stage l	Pa
$T_{a,l}$	Inflow temperature at stage l	K
$q_{a(l,k)}$	Mass flow through unit k at stage l	$\mathrm{kg\,s^{-1}}$
$q^{\mathrm{fuel}}_{a(l,k)}$	Fuel consumption of compressor unit k at stage l	$\mathrm{kg\,s^{-1}}$
q^{fuel}_{a}	Fuel consumption of the station	$\mathrm{kg\,s^{-1}}$

TABLE 4. Notation for the compressor station model.

To fix some notation, we number the serial stages with $l = 1, \ldots, s$ and the compressor units at stage l with $k = 1, \ldots, m_l$, where stage l connects nodes l and $l+1$. An overview of physical and technical quantities and our notation for compressor stations is given in Table 4. At every stage the flow divides over the parallel units:

$$q_a = \sum_{k=1}^{m_l} q_{a(l,k)}, \quad l = 1, \ldots, s. \tag{62}$$

The inflow pressures $p_{a,l}$ and $p_{a,l+1}$ at stages $l, l+1$ are identical to the common inflow and outflow pressures of all parallel units at stage l, respectively:

$$p_{a,l} = p_{i(l,k)}, \qquad l = 1, \ldots, s, \quad k = 1, \ldots, m_l, \tag{63}$$

$$p_{a,l+1} = p_{j(l,k)}, \qquad l = 1, \ldots, s, \quad k = 1, \ldots, m_l. \tag{64}$$

The same holds for the gas temperature except that the outflow temperatures of parallel units do not have to be equal. We assume perfect mixing again, yielding a common averaged inflow temperature at the next stage:

$$T_{i(l,k)} = T_{a,l}, \qquad l = 1, \ldots, s, \quad k = 1, \ldots, m_l, \tag{65}$$

$$\frac{\sum_{k=1}^{m_l} q_{a(l,k)} T_{j(l,k)}}{\sum_{k=1}^{m_l} q_{a(l,k)}} = T_{a,l+1}, \qquad l = 1, \ldots, s. \tag{66}$$

The temperature averaging equation is consistent with (9) since the gas composition does not change within the station and hence the molar mass factors cancel each other.

For a model of the complete station we regard the inflow resistor, outflow resistor, gas cooler and station exit as respective stages 0, $s+1$, $s+2$ and $s+3$ (see Fig. 7). The station inflow pressure, $p_i \equiv p_{a,0}$, is thus reduced by the inflow resistor yielding $p_{a,1}$, and similarly the outflow resistor reduces $p_{a,s+1}$, yielding $p_{a,s+2} = p_{a,s+3} \equiv p_j$ (the gas cooler does not influence the pressure). The pressure losses at the two resistors cause corresponding temperature losses from $T_{a:i} \equiv T_{a,0}$ to $T_{a,1}$ and from $T_{a,s+1}$ to $T_{a,s+2}$. In addition, the gas cooler restricts the station outflow temperature to a given maximum T_a^+,

$$T_j \equiv T_{a,s+3} = \min(T_{a,s+2}, T_a^+). \tag{67}$$

Symbol	Explanation	Unit
H_{ad}	Adiabatic head	$\mathrm{J\,kg^{-1}}$
n	Compressor speed	$\mathrm{s^{-1}}$
P	Compressor input power	W
η_{ad}	Adiabatic efficiency	1
κ	Isentropic exponent	1
V_o	Operating volume of piston compressor	$\mathrm{m^3}$
M	Shaft torque of piston compressor	N m

TABLE 5. Physical and technical quantities of compressor machines.

To avoid nonsmoothness, we replace (67) with the uniformly convergent approximation (14):

$$T_j = T_a^+ - \frac{1}{2}\left(\sqrt{\Delta T_a^2 + \epsilon} - \Delta T_a\right), \quad \Delta T_a = T_{a,s+2} - T_a^+. \tag{68}$$

The gas cooler consumes a tiny amount of the compressed gas, which we neglect for simplicity.

Finally we obtain the fuel consumption of the compressor station as the sum of fuel consumptions of all active compressor units:

$$q_a^{\mathrm{fuel}} = \sum_{l=1}^{s}\sum_{k=1}^{m_l} q_{a(l,k)}^{\mathrm{fuel}}. \tag{69}$$

3.4.10. *Compressors.* The main physical process in a compressor unit of any type is the adiabatic compression of gas, i.e., the increase of gas pressure without heat transfer (see Table 5 for the notation). The associated adiabatic head measures the energy required for compression of a unit mass of gas; it depends on the inflow temperature T_{in} and the compression ratio $p_{\mathrm{out}}/p_{\mathrm{in}}$ [13]:

$$H_{\mathrm{ad}}(T_{\mathrm{in}}, T_{\mathrm{out}}, p_{\mathrm{in}}, p_{\mathrm{out}}) = \frac{z_{\mathrm{in}} T_{\mathrm{in}}}{\gamma_0}\frac{\kappa}{\kappa - 1}\left(\left(\frac{p_{\mathrm{out}}}{p_{\mathrm{in}}}\right)^{(\kappa-1)/\kappa} - 1\right), \quad \kappa = \kappa(T_{\mathrm{in}}, T_{\mathrm{out}}, p_{\mathrm{in}}, p_{\mathrm{out}}). \tag{70}$$

Here $T_{\mathrm{in}}, T_{\mathrm{out}}, p_{\mathrm{in}}, p_{\mathrm{out}}$ correspond to $T_{i(l,k)}, T_{j(l,k)}, p_{a,l}, p_{a,l+1}$ in the station model if we are considering compressor $a(l,k)$. The compression process is adiabatic and reversible, hence isentropic. The isentropic exponent κ depends on the pressures and temperatures during the entire process; several approximations exist that differ in complexity and accuracy [37]. The most accurate model defines $\kappa = \frac{1}{2}(\kappa_{\mathrm{in}} + \kappa_{\mathrm{out}})$ where $\kappa_{\mathrm{in}}, \kappa_{\mathrm{out}}$ are obtained by substituting $(p_{\mathrm{in}}, T_{\mathrm{in}})$ and $(p_{\mathrm{out}}, T_{\mathrm{out}})$ into the following equation:

$$\kappa(p,T) = \frac{z}{Z_p - Z_T^2/(\gamma_0 c_p)}, \quad Z_p(p,T) = z - p\frac{\partial z}{\partial p}, \quad Z_T(p,T) = z + T\frac{\partial z}{\partial T}. \tag{71}$$

A simpler formula neglecting the pressure dependence defines κ as a function of the "mean" temperature T_m,

$$\kappa(T_m) = 1.29 - c(T_m - T_0), \quad T_m = \frac{1}{2}(T_{\mathrm{in}} + T_{\mathrm{out}}), \quad c = 5.8824 \times 10^{-4}\ \mathrm{K^{-1}}. \tag{72}$$

Even simpler, the constant value $\kappa = 1.29$ is often used in practice, which is obtained from (72) with $T_m = T_0$.

Next we consider the power required at operating conditions $(Q, T_{\mathrm{in}}, p_{\mathrm{in}}, p_{\mathrm{out}})$. The compressor output power (transmitted to the gas) is qH_{ad}, yielding with the adiabatic efficiency η_{ad} the compressor input power

$$P = \frac{qH_{\mathrm{ad}}}{\eta_{\mathrm{ad}}}. \tag{73}$$

This power is delivered by a corresponding drive $d = \sigma(a) \in \mathbb{D}$, where $\mathbb{A}_{\mathrm{cu}}, \mathbb{D}$ denote the sets of all compressor units and drives, respectively, and $\sigma\colon \mathbb{A}_{\mathrm{cu}} \to \mathbb{D}$ associates a drive d to every compressor

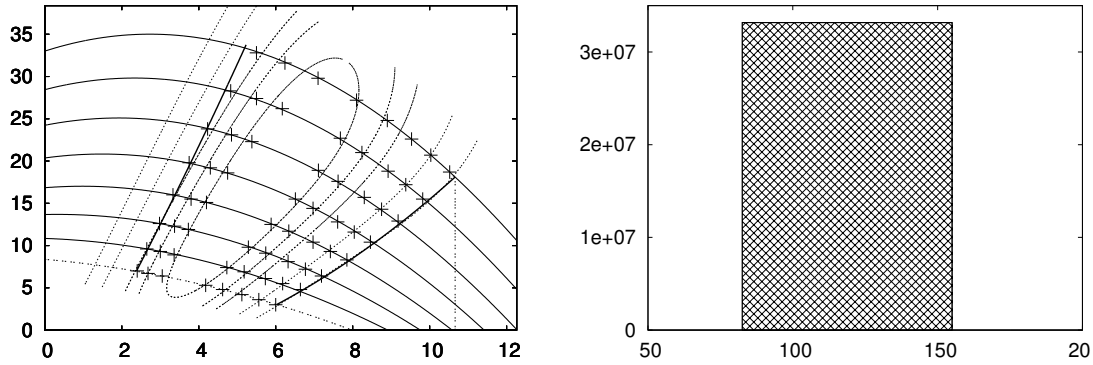

FIGURE 9. Characteristic diagrams of turbo compressor (left; adiabatic head vs. volumetric flow) and piston compressor (right; shaft torque vs. volumetric flow). The turbo compressor is characterized by its isolines for speed (solid; decreasing from top to bottom) and adiabatic efficiency (dashed; decreasing from center to borders). The maximal shaft torque of a piston compressor is independent of the flow rate but may depend on the inflow pressure, see (84).

unit e. The compressor drive limits the input power,

$$P \le P_d^+. \tag{74}$$

It also determines the fuel consumption

$$q^{\text{fuel}} = \frac{b_d \rho_0}{H_u}, \tag{75}$$

where b_d is the specific energy consumption rate of the drive and $H_u = cH_c$ is the lower calorific value of the gas, a constant fraction of the higher calorific value H_c. A detailed model of drives will be given in Sect. 3.4.15.

3.4.11. *Turbo Compressors.* In this section we consider various data fits based on bivariate and univariate quadratic polynomials. These are generically denoted as $\chi(x, y; A)$ and $\psi(z; b)$ with coefficients $A \in \mathbb{R}^{3\times 3}$ or $b \in \mathbb{R}^3$:

$$\chi(x,y;A) = \begin{pmatrix} 1 \\ x \\ x^2 \end{pmatrix}^T \begin{bmatrix} a_{00} & a_{01} & a_{02} \\ a_{10} & a_{11} & a_{12} \\ a_{20} & a_{12} & a_{22} \end{bmatrix} \begin{pmatrix} 1 \\ y \\ y^2 \end{pmatrix}, \quad \psi(z;b) = \begin{pmatrix} b_0 \\ b_1 \\ b_2 \end{pmatrix}^T \begin{pmatrix} 1 \\ z \\ z^2 \end{pmatrix}. \tag{76}$$

If the coefficients are not of interest we simply write $\chi(x, y)$ and $\psi(z)$.

Turbo compressors are the most complicated machines in compressor stations. Their technical behavior is described by *characteristic diagrams* (see Fig. 9) where the coordinates are adiabatic head H_{ad} (y axis) and volumetric flow Q before compression (x axis), i.e., $Q = q/\rho_{\text{in}}$. Again, we drop the index e for better reading. The technical properties of turbo compressors are given by a set of functions representing certain lines in the characteristic diagram: first, the set of isolines for speed, $H_{\text{ad}}(Q, n) = \chi(Q, n; A_{H_{\text{ad}}})$; second, the set of isolines of adiabatic efficiency, $\eta_{\text{ad}}(Q, n) = \chi(Q, n; A_{\eta_{\text{ad}}})$. The "+" symbols in the characteristic diagram indicate measured data of the specific machine to which the coefficients are fitted. Together with the speed bounds $n \in [n^-, n^+]$, the *surgeline* $\mathcal{S} = \{(Q, H_{\text{ad}})\colon \psi(Q; b_s) = H_{\text{ad}}\}$ (left bold line) and the *chokeline* $\mathcal{C} = \{(Q, H_{\text{ad}})\colon \psi(Q; b_c) = H_{\text{ad}}\}$ (right bold line), one has a complete description of the operating range of the machine. In summary, the characteristic diagram is modeled by a system of nonlinear

equations and inequalities:

$$H_{\mathrm{ad}}(Q,n) = \chi(Q,n;A_{H_{\mathrm{ad}}}), \tag{77}$$

$$\eta_{\mathrm{ad}}(Q,n) = \chi(Q,n;A_{\eta_{\mathrm{ad}}}), \tag{78}$$

$$n \in [n^-, n^+], \tag{79}$$

$$\mathcal{S}\colon\ \psi(Q;b_s) \geq H_{\mathrm{ad}}, \tag{80}$$

$$\mathcal{C}\colon\ \psi(Q;b_c) \leq H_{\mathrm{ad}}. \tag{81}$$

In practice, the curved chokeline constraint is sometimes replaced with a fixed upper bound Q^+ on the volumetric flow through the machine, defined by the intersection point of $\mathcal{C}$ and $H_{\mathrm{ad}}(Q,n^+)$. This increases the feasible region at the cost of allowing otherwise undesired operation of the unit at very low efficiency, $\eta_{\mathrm{ad}}(Q,n) \ll 1$.

3.4.12. *Piston Compressors.* A less common type of compressors are piston compressors, which yield larger compression ratios but less throughput than turbo compressors. Piston compressors are also described by characteristic diagrams, where the coordinates are now volumetric flow Q and shaft torque M, see Fig. 9.

The volumetric flow through a piston compressor is the product of its operating volume V_o (compressed during one revolution) and the speed,

$$Q = V_o n \in [V_o n^-, V_o n^+]. \tag{82}$$

The shaft torque is defined by

$$M = \frac{V_o H_{\mathrm{ad}}}{2\pi\eta_{\mathrm{ad}}}\rho_{\mathrm{in}}, \tag{83}$$

where η_{ad} is a machine-dependent constant. Finally, piston compressors have a limitation of the compression ratio. Depending on the technical data supplied with a specific unit, this limitation is given in one of the following forms:

$$\frac{p_{\mathrm{out}}}{p_{\mathrm{in}}} \leq \varepsilon^+, \quad p_{\mathrm{out}} \leq p_{\mathrm{in}} + \Delta p^+, \quad M \leq M^+. \tag{84}$$

3.4.13. *Idealized Compressor Model.* Earlier approaches to gas network optimization often consider *idealized* models of compressor units and drives, see, e.g., [18, 60, 42, 40, 43, 44]. We also use them if possible; however, it turns out that this is rarely appropriate [54]. These idealized models incorporate the basic physical relations shared by turbo and piston compressors: adiabatic head (70), power consumption (73), and fuel consumption (75). However, they assume a constant adiabatic efficiency and they replace characteristic diagrams and drive properties with a constant fuel consumption rate $b_{\sigma(a)}$ and with simple bounds on the compressor input power,

$$P \in [P^-, P^+]. \tag{85}$$

3.4.14. *Temperature Increase.* The compression of gas increases its temperature. This effect is modeled in two stages [37]: the temperature increase of ideal gas first defines $T_{\mathrm{out}}^{\mathrm{ideal}}$, then this value is used to initialize a fixed point iteration for T_{out},

$$T_{\mathrm{out}}^{(k+1)} = T_{\mathrm{out}}^{\mathrm{ideal}} \frac{z(p_{\mathrm{in}}, T_{\mathrm{in}})}{z(p_{\mathrm{out}}, T_{\mathrm{out}}^{(k)})}, \quad T_{\mathrm{out}}^{(0)} = T_{\mathrm{out}}^{\mathrm{ideal}}, \quad k = 0, 1, 2, \ldots \tag{86}$$

We consider three different models for $T_{\mathrm{out}}^{\mathrm{ideal}}$:

$$T_{\mathrm{out}}^{\mathrm{ideal}} = T_{\mathrm{in}} \left(\frac{p_{\mathrm{out}}}{p_{\mathrm{in}}}\right)^{(\kappa-1)/\kappa}, \tag{87}$$

$$T_{\mathrm{out}}^{\mathrm{ideal}} = T_{\mathrm{in}} \left(\frac{p_{\mathrm{out}}}{p_{\mathrm{in}}}\right)^{(\kappa-1)/(\kappa\eta_{\mathrm{ad}})}, \tag{88}$$

$$T_{\mathrm{out}}^{\mathrm{ideal}} = T_{\mathrm{in}} \left(\frac{1}{\eta_{\mathrm{ad}}} \left(\left(\frac{p_{\mathrm{out}}}{p_{\mathrm{in}}}\right)^{(\kappa-1)/\kappa} - 1\right) + 1\right). \tag{89}$$

Symbol	Explanation	Unit
P^+	Maximal power to provide for the compressor unit	W
b	Specific energy consumption rate	W
T_{amb}	Ambient temperature at the compressor station	K

TABLE 6. Notation for drive models.

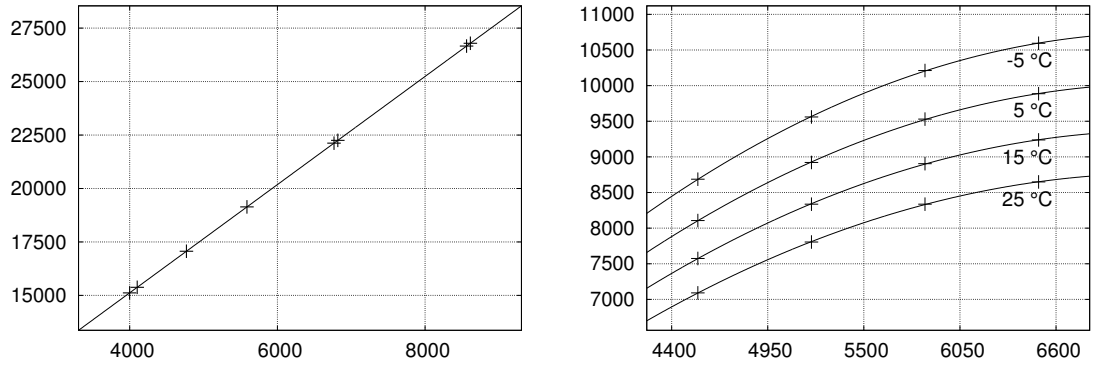

FIGURE 10. Characteristic diagrams of a gas turbine: specific energy consumption rate (kW) vs. power (kW, left) and maximal power vs. speed (min^{-1}, right).

Equation (89) can also be found in [57]. Three prominent models from the literature each combine a certain number ℓ of fixed point iterations with one of these initializations:

(90) isentropic equation model: (87) with $\ell = 0$,

(91) standard model: (88) with $\ell = 1$,

(92) RG1991 model: (89) with $\ell = \infty$ (ℓ determined adaptively).

3.4.15. *Compressor Drives.* Compressor drives provide the compressor units with power. They are operated either with fuel gas from the network or with electricity. In our model, the drives are not elements of the graph G but are only coupled with the network by the mapping $\sigma\colon \mathbb{A}_{\text{cu}} \to \mathbb{D}$. For the notation see Table 6. We distinguish four drive types: gas turbines $\mathbb{D}_{\text{gt}}$, gas driven motors $\mathbb{D}_{\text{gm}}$, steam turbines $\mathbb{D}_{\text{st}}$, and electric motors $\mathbb{D}_{\text{em}}$,

$$\mathbb{D} = \mathbb{D}_{\text{gt}} \cup \mathbb{D}_{\text{gm}} \cup \mathbb{D}_{\text{st}} \cup \mathbb{D}_{\text{em}}. \tag{93}$$

The four types are described in the following, where drive d is associated with compressor e.

Gas turbines are specified by two characteristic diagrams: the maximal power depending on speed and ambient temperature, $P_d^+(n_a, T_{\text{amb}}) = \chi(n_a, T_{\text{amb}}; A_{P_d^+})$, and the specific energy consumption rate $b_d(P_a) = \psi(P_a; b_{b_d})$, see Fig. 10.

Gas driven motors are similar to gas turbines, except that the dependence of their maximal power on the ambient temperature is considered to be negligible: $P_d^+(n_a) = \psi(n_a; b_{P_d^+})$.

Steam turbines have fixed power bounds rather than a maximal power function: $P_a \in [P_d^-, P_d^+]$. The fuel consumption is modeled as in gas turbines.

Electric motors consume as much electric power as they deliver to the compressor, P_a, and hence do not have a fuel consumption model. Depending on the specific drive, the maximal power function may or may not depend on the ambient temperature (sets $\mathbb{D}_{\text{em},1}$ and $\mathbb{D}_{\text{em},0}$).

Symbol	Explanation	Unit
Δp	Pressure decrease	Pa
μ_{JT}	Joule–Thomson coefficient	$\mathrm{K\,Pa^{-1}}$

TABLE 7. Notation for the control valve station model.

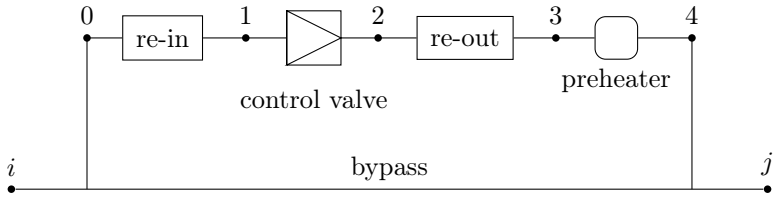

FIGURE 11. Control valve station (schematic overview).

In summary, a generic drive model encompassing all cases can be stated as

$$b_d(P_a) = \psi(P_a), \quad d \in \mathbb{D}_{\mathrm{gt}} \cup \mathbb{D}_{\mathrm{gm}} \cup \mathbb{D}_{\mathrm{st}}, \tag{94}$$

$$P_d^+(n_a, T_{\mathrm{amb}}) = \chi(n_a, T_{\mathrm{amb}}), \quad d \in \mathbb{D}_{\mathrm{gt}} \cup \mathbb{D}_{\mathrm{em},1}, \tag{95}$$

$$P_d^+(n_a) = \psi(n_a), \quad d \in \mathbb{D}_{\mathrm{gm}} \cup \mathbb{D}_{\mathrm{em},0}, \tag{96}$$

$$P_d^{\pm} \text{ given}, \quad d \in \mathbb{D}_{\mathrm{st}}. \tag{97}$$

We finally mention that two compressors may be mounted on a single drive shaft. In this case they have identical speeds and their combined power consumption is bounded by the drive's limit.

3.4.16. *Control Valve Stations.* Like compressor stations, control valve stations $a = ij \in \mathbb{E}_{\mathrm{cv}}$ can be operated in three modes: closed, bypass and active, where closed and bypass modes are exactly identical to the respective compressor station modes. An *active* station reduces the gas pressure by a controlled and bounded amount. The effects of station piping, filters, etc., are again modeled as inflow and outflow resistors, but at the station exit we now have a gas preheater, see Fig. 11.

We regard the control valve itself as stage 1 and the resistors and preheater as stages 0, 2, 3. The controlled pressure reduction of stage 1 is modeled as

$$p_{a,2} = p_{a,1} - \Delta p_a, \quad \Delta p_a \in [\Delta p_a^-, \Delta p_a^+], \tag{98}$$

where Δp_a^- is zero in most cases. The Joule–Thomson effect causes a corresponding reduction of the gas temperature obtained as an ODE solution involving the Joule–Thomson coefficient μ_{JT}:

$$T_{a,2} - T_{a,1} = \int_{p_{a,1}}^{p_{a,2}} \mu_{\mathrm{JT}}(p,T)\,\mathrm{d}p, \quad \mu_{\mathrm{JT}}(p,T) = \frac{T}{p}\frac{R}{\tilde{c}_p}(Z_T - z). \tag{99}$$

Here R is the universal gas constant, $\tilde{c}_p = c_p m$ is the molar heat capacity, and Z_T is defined as in (71). Our computational experiments (cf. [54]) show that a single implicit Euler step is sufficiently accurate in this context:

$$\frac{T_{a,2} - T_{a,1}}{p_{a,2} - p_{a,1}} = \mu_{\mathrm{JT}}(p_{a,2}, T_{a,2}) = \frac{T_{a,2}}{p_{a,2}}\frac{R}{\tilde{c}_{p,2}}(Z_{T,2} - z_{a,2}). \tag{100}$$

Here all quantities with index 2 correspond to outflow conditions at stage 1. If we rewrite (100) as

$$T_{a,2} - T_{a,1} = \omega_a(p_{a,2} - p_{a,1}), \quad \omega_a = \mu_{\mathrm{JT}}(p_{a,2}, T_{a,2}), \tag{101}$$

we may even obtain a linear approximation by assuming ω_a to be a suitable constant.

If the temperature loss caused by the Joule–Thomson effect is too large, the *gas preheater* is activated to keep the gas temperature above a given minimum T_a^-:

$$T_{a:j} \equiv T_{a,4} = \max(T_{a,3}, T_a^-). \tag{102}$$

Here we avoid nonsmoothness by using the uniformly convergent approximation (15),

$$T_{a,4} = T_a^- + \frac{1}{2}\left(\sqrt{\Delta T_a^2 + \epsilon} + \Delta T_a\right), \quad \Delta T_a = T_{a,3} - T_a^-. \tag{103}$$

Like gas coolers, the preheaters consume a tiny amount of gas that we neglect.

3.4.17. *Control Valves Without Remote Access.* Control valves without remote access are control valve stations with an automated state-dependent mode of operation: their control is designed to keep the outgoing pressure below a given threshold, $p_j \le p_j^{\mathrm{set}}$. Again we need to take in- and outgoing resistors into account, with further pressure losses Δp_{in} and Δp_{out} according to (11) or (12). In our stationary model the control valve without remote access is in bypass mode if $p_i - \Delta p_{\mathrm{in}} - \Delta p_{\mathrm{out}} \le p_j^{\mathrm{set}}$. The station closes automatically when the outflow pressure cannot be kept below the threshold, $p_i - \Delta p_{\mathrm{in}} - \Delta p_{\mathrm{out}} > p_j^{\mathrm{set}} + \Delta p_a^+$. Otherwise the element is active, reducing the pressure by some amount $\Delta p_a \in [0, \Delta p_a^+]$ so that $p_j = p_j^{\mathrm{set}}$.

From an optimization perspective, control valves without remote access are *passive* elements: they are not controllable by the network dispatchers; rather, they implement a (nonsmooth) functional dependence of the outflow pressure on the inflow pressure.

3.5. **Objective.** Various objectives may be appropriate depending on the specific planning problem under consideration. For concreteness we present the minimization of variable operating costs, which is the natural objective in operative planning:

$$\min \sum_{a \in \mathbb{A}_{\mathrm{cu}}^{\mathrm{gas}}} c_a^{\mathrm{fuel}} q_a^{\mathrm{fuel}} + \sum_{a \in \mathbb{A}_{\mathrm{cu}}^{\mathrm{el}}} c_a^{\mathrm{el}} P_a. \tag{104}$$

Here $c_a^{\mathrm{fuel}}, c_a^{\mathrm{el}}$ are the specific fuel consumption and electricity costs, and $\mathbb{A}_{\mathrm{cu}}^{\mathrm{gas}}, \mathbb{A}_{\mathrm{cu}}^{\mathrm{el}}$ denote the respective sets of gas-driven and electricity-driven compressor units,

$$\mathbb{A}_{\mathrm{cu}}^{\mathrm{gas}} = \{a \in \mathbb{A}_{\mathrm{cu}} \colon \sigma(a) \in \mathbb{D} \setminus \mathbb{D}_{\mathrm{em}}\}, \qquad \mathbb{A}_{\mathrm{cu}}^{\mathrm{el}} = \{a \in \mathbb{A}_{\mathrm{cu}} \colon \sigma(a) \in \mathbb{D}_{\mathrm{em}}\}.$$

4. Outlook

The hierarchies of model components for natural gas networks presented here can be combined in various ways to obtain complete NLP type models. In part 2 of this paper [54] we will provide validations of the component models based on comparisons with a commercial simulation package. We will also develop special techniques for handling various nonsmooth model aspects, discuss the interaction of our models and techniques with preceding mixed-integer optimization steps, and finally present results of the overall approach for real gas networks.

References

[1] P. Bales, *Hierarchische Modellierung der Eulerschen Flussgleichungen in der Gasdynamik*, Master's thesis, Technische Universität Darmstadt, 2005.

[2] M. K. Banda and M. Herty, *Multiscale modeling for gas flow in pipe networks*, Mathematical Methods in the Applied Sciences, 31 (2008), pp. 915–936.

[3] M. K. Banda, M. Herty, and A. Klar, *Gas flow in pipeline networks*, Networks and Heterogeneous Media, 1 (2006), pp. 41–56.

[4] C. Borraz-Sánchez and R. Z. Ríos-Mercado, *A procedure for finding initial feasible solutions on cyclic natural gas networks*, in Proceedings of the 2004 NSF Design, Service and Manufacturing Grantees and Research Conference, Dallas, USA, January 2004.

[5] ———, *A Hybrid Meta-Heuristic Approach for Natural Gas Pipeline Network Optimization*, in Hybrid Metaheuristics, M. Blesa, C. Blum, A. Roli, and M. Sampels, eds., vol. 3636 of Lecture Notes in Computer Science, Springer, 2005, pp. 54–65. http://dx.doi.org/10.1007/11546245_6.

[6] E. A. Boyd, L. R. Scott, and S. Wu, *Evaluating the quality of pipeline optimization algorithms*, in PSIG 29th Annual Meeting, Tucson, Arizona, Pipeline Simulation Interest Group, 1997. Paper 9709.

[7] J. Brouwer, I. Gasser, and M. Herty, *Gas pipeline models revisited: Model hierarchies, nonisothermal models, and simulations of networks*, Multiscale Model. Simul., 9 (2011), pp. 601–623.

[8] J. Burgschweiger, B. Gnädig, and M. C. Steinbach, *Optimization models for operative planning in drinking water networks*, Optim. Eng., 10 (2009), pp. 43–73. Published online 2008.

[9] J. Burgschweiger, B. Gnädig, and M. C. Steinbach, *Nonlinear programming techniques for operative planning in large drinking water networks*, The Open Appl. Math. J., 3 (2009), pp. 14–28.

[10] R. G. Carter, *Compressor station optimization: Computational accuracy and speed*, in 28th Annual Meeting, Pipeline Simulation Interest Group, 1996. Paper 9605.
[11] ———, *Pipeline optimization: Dynamic Programming after 30 years*, in 30th Annual Meeting, Pipeline Simulation Interest Group, 1998. Paper 9803.
[12] R. G. Carter, D. W. Schroeder, and T. D. Harbick, *Some Causes and Effects of Discontinuities in Modeling and Optimizing Gas Transmission Networks*, tech. rep., Stoner Associates, Carlisle, PA, USA, Apr. 1994.
[13] G. Cerbe, *Grundlagen der Gastechnik*, Hanser, 2008.
[14] D. Cobos-Zaleta and R. Z. Ríos-Mercado, *A MINLP model for a problem of minimizing fuel consumption on natural gas pipeline networks*, in Proc. XI Latin-Ibero-American Conference on Operations Research, 2002, pp. 1–9. Paper A48-01.
[15] D. de Wolf and Y. Smeers, *The gas transmission problem solved by an extension of the simplex algorithm*, Management Sci., 46 (2000), pp. 1454–1465.
[16] P. Domschke, B. Geissler, O. Kolb, J. Lang, A. Martin, and A. Morsi, *Comparison of nonlinear and linear optimization of transient gas networks*, INFORMS Journal of Computing, (2010), pp. 1–13.
[17] K. Ehrhardt and M. C. Steinbach, *KKT systems in operative planning for gas distribution networks*, Proc. Appl. Math. Mech., 4 (2004), pp. 606–607.
[18] ———, *Nonlinear optimization in gas networks*, in Modeling, Simulation and Optimization of Complex Processes, H. G. Bock, E. Kostina, H. X. Phu, and R. Rannacher, eds., Springer, Berlin, 2005, pp. 139–148.
[19] M. Feistauer, *Mathematical Methods in Fluid Dynamics*, vol. 67 of Pitman Monographs and Surveys in Pure and Applied Mathematics Series, Longman Scientific & Technical, Harlow, 1993.
[20] E. J. Finnemore and J. E. Franzini, *Fluid Mechanics wth Engineering Applications*, McGraw-Hill, 10th ed., 2002.
[21] A. Fügenschuh, B. Geissler, N. Geissler, R. Gollmer, B. Hiller, J. Humpola, T. Koch, T. Lehmann, A. Martin, A. Morsi, M. Pfetsch, J. Rövekamp, L. Schewe, M. Schmidt, R. Schultz, R. Schwarz, J. Schweiger, C. Stangl, M. C. Steinbach, S. Vigerske, and B. M. Willert, *The validation of nominations in gas network optimization: Models, methods, and solutions*. In preparation.
[22] A. Fügenschuh, B. Geissler, R. Gollmer, C. Hayn, R. Henrion, B. Hiller, J. Humpola, T. Koch, T. Lehmann, A. Martin, R. Mirkov, A. Morsi, M. Pfetsch, L. Schewe, M. Schmidt, R. Schultz, R. Schwarz, J. Schweiger, C. Stangl, M. C. Steinbach, S. Vigerske, and B. M. Willert, *From simulation to optimization: Evaluating gas network capacities*. In preparation for MOS-SIAM Series on Optimization.
[23] A. Fügenschuh, B. Geissler, R. Gollmer, C. Hayn, R. Henrion, B. Hiller, J. Humpola, T. Koch, T. Lehmann, A. Martin, R. Mirkov, W. Römisch, J. Rövekamp, L. Schewe, M. Schmidt, R. Schultz, R. Schwarz, J. Schweiger, C. Stangl, M. C. Steinbach, and B. M. Willert, *Mathematical optimization for challenging network planning problems in unbundled gas markets*. In preparation.
[24] P. E. Gill, W. Murray, and M. S. Saunders, *SNOPT: An SQP algorithm for large-scale constrained optimization*, SIAM J. Optim., 12 (2002), pp. 979–1006.
[25] M. Gugat, *Boundary controllability between sub- and supercritical flow*, SIAM J. Control Optim., 42 (2003), pp. 1056–1070.
[26] M. Gugat and G. Leugering, *Global boundary controllability of the de St. Venant equations between steady states*, Annales de l'Institut Henri Poincare (C) Non Linear Analysis, 20 (2003), pp. 1 – 11.
[27] M. Gugat, G. Leugering, K. Schittkowski, and E. J. P. G. Schmidt, *Modelling, stabilization, and control of flow in networks of open channels*, in Online Optimization of Large Scale Systems, M. Grötschel, S. O. Krumke, and J. Rambau, eds., Springer, Berlin, 2001, pp. 251–270.
[28] P. Hackländer, *Integrierte Betriebsplanung von Gasversorgungssystemen*, Ph. D. dissertation, Universität Wuppertal, 2002.
[29] T. Jeníček, *Steady-state optimization of gas transport*, in SIMONE [58], pp. 26–38.
[30] T. Jeníček, J. Králik, J. Štěrba, Z. Vostrý, and J. Záworka, *Study to analyze the possibilities and features of an optimization system (optimum control system) to support the dispatching activities of Ruhrgas*. Vertrauliche Dokumentation, LIWACOM Informationstechnik GmbH Essen, 1993.
[31] D. L. V. Katz, *Handbook of natural gas engineering*, McGraw-Hill series in chemical engineering, McGraw-Hill, 1959.
[32] J. Králik, *Compressor stations in SIMONE*, in SIMONE [58], pp. 93–117.
[33] J. Králik, P. Stiegler, Z. Vostrý, and J. Závorka, *A universal dynamic simulation model of gas pipeline networks*, IEEE Trans. Syst., Man, Cybern., 14 (1984), pp. 597–606.
[34] J. Králik, P. Stiegler, Z. Vostrý, and J. Záworka, *Modeling the dynamics of flow in gas pipelines*, IEEE Trans. Syst., Man, Cybern., SMC-14 (1984), pp. 586–596.
[35] O. Kunz, R. Klimeck, W. Wagner, and M. Jaeschke, *The GERG-2004 Wide-Range Equation of State for Natural Gases and Other Mixtures*, no. 557 in Fortschritt-Berichte VDI, Reihe 6, VDI Verlag, Düsseldorf, 2007. GERG Technical Monograph 15.
[36] G. Leugering and E. J. P. G. Schmidt, *On the modelling and stabilization of flows in networks of open canals*, SIAM J. Control Optim., 41 (2002), pp. 164–180.

[37] LIWACOM Informations GmbH and SIMONE Research Group s.r.o., *Gleichungen und Methoden*, 2004. Benutzerhandbuch.
[38] M. V. Lurie, *Modeling of Oil Product and Gas Pipeline Transportation*, Wiley-VCH, 2008.
[39] A. Martin, B. Geissler, C. Hayn, B. Hiller, J. Humpola, T. Koch, T. Lehmann, A. Morsi, M. Pfetsch, L. Schewe, M. Schmidt, R. Schultz, R. Schwarz, J. Schweiger, M. C. Steinbach, and B. M. Willert, *Optimierung Technischer Kapazitäten in Gasnetzen*, in Optimierung in der Energiewirtschaft, vol. 2157 of VDI-Berichte, 2011, pp. 105–114.
[40] A. Martin, D. Mahlke, and S. Moritz, *A simulated annealing algorithm for transient optimization in gas networks*, Math. Methods Oper. Res., 66 (2007), pp. 99–115.
[41] A. Martin and M. Möller, *Cutting planes for the optimization of gas networks*, in Modeling, Simulation and Optimization of Complex Processes, H. G. Bock, E. Kostina, H. X. Phu, and R. Rannacher, eds., Springer, Berlin, 2005, pp. 307–329.
[42] A. Martin, M. Möller, and S. Moritz, *Mixed integer models for the stationary case of gas network optimization*, Math. Program., 105 (2006), pp. 563–582.
[43] M. Möller, *Mixed Integer Models for the Optimisation of Gas Networks in the Stationary Case*, Ph. D. dissertation, Technische Universität Darmstadt, 2004.
[44] S. Moritz, *A Mixed Integer Approach for the Transient Case of Gas Network Optimization*, Ph. D. dissertation, Technische Universität Darmstadt, 2007.
[45] F. M. Odom and G. L. Muster, *Tutorial on modeling of gas turbine driven centrifugal compressors*, Tech. Rep. 09A4, Pipeline Simulation Interest Group, 2009.
[46] A. Osiadacz, *Nonlinear programming applied to the optimum control of a gas compressor station*, Int. J. Numer. Methods Eng., 15 (1980), pp. 1287–1301.
[47] D. Oucherif, *Approximation der stationären Impulsgleichung realer Gase in Pipelines*, Master's thesis, Leibniz Universität Hannover, 2009.
[48] I. Papay, *OGIL Musz. Tud. Kozl.*, 1968.
[49] K. F. Pratt and J. G. Wilson, *Optimization of the operation of gas transmission systems*, Transactions of the Institute of Measurement and Control, 6 (1984), pp. 261–269.
[50] O. Redlich and J. N. S. Kwong, *On the Thermodynamics of Solutions. V. An Equation of State. Fugacities of Gaseous Solutions*, Chemical Reviews, 44 (1949), pp. 233–244. PMID: 18125401.
[51] R. Z. Ríos-Mercado, S. Kim, and A. E. Boyd, *Efficient operation of natural gas transmission systems: A network-based heuristic for cyclic structures*, Computers & Operations Research, 33 (2006), pp. 2323–2351.
[52] R. Z. Ríos-Mercado, S. Wu, L. R. Scott, and A. E. Boyd, *A reduction technique for natural gas transmission network optimization problems*, Ann. Oper. Res., 117 (2002), pp. 217–234.
[53] J. Saleh, ed., *Fluid Flow Handbook*, McGraw-Hill Handbooks, McGraw-Hill, 2002.
[54] M. Schmidt, M. C. Steinbach, and B. M. Willert, *High detail stationary optimization models for gas networks — Part 2: Validation and results.* In preparation.
[55] ———, *A smoothed and relaxed MPEC approach to MINLP for gas networks.* In preparation.
[56] E. Sekirnjak, *Mixed integer optimization for gas transmission and distribution systems.* Vortragsmanuskript, INFORMS-Meeting, Seattle, Oct. 1998.
[57] ———, *Transiente Technische Optimierung (TTO-Prototyp).* Vertrauliche Dokumentation, PSI AG, Berlin, 1999.
[58] *Proceedings of 2nd International Workshop SIMONE on Innovative Approaches to Modeling and Optimal Control of Large Scale Pipeline Networks*, Prague, 1993.
[59] K. Starling and J. Savidge, *Compressibility factors of natural gas and other related hydrocarbon gases*, Transmission Measurement Committee report, AGA, American Gas Association, 1992.
[60] M. C. Steinbach, *On PDE solution in transient optimization of gas networks*, J. Comput. Appl. Math., 203 (2007), pp. 345–361.
[61] T. van der Hoeven, *Math in Gas and the art of linearization*, PhD thesis, Rijksuniversiteit Groningen, 2004.
[62] Y. Villalobos-Morales, D. Cobos-Zaleta, H. J. Flores-Villarreal, C. Borraz-Sánchez, and R. Z. Ríos-Mercado, *On NLP and MINLP Formulations and Preprocessing for Fuel Cost Minimization of Natural Gas Transmission Networks*, in Proceedings of the 2003 NSF Design, Service and Manufacturing Grantees and Research Conference, Birmingham, USA, January 2003.
[63] Z. Vostrý, *Transient optimization of gas transport and distribution*, in SIMONE [58], pp. 53–62.
[64] A. Wächter and L. T. Biegler, *On the implementation of an interior-point filter line-search algorithm for large-scale nonlinear programming*, Math. Program., 106 (2006), pp. 25–57.
[65] A. Weimann, *Modellierung und Simulation der Dynamik von Gasnetzen im Hinblick auf Gasnetzführung und Gasnetzüberwachung*, Ph. D. dissertation, Technische Universität München, 1978.
[66] T. R. Weymouth, *Problems in Natural Gas Engineering*, Transactions of the American Society of Mechanical Engineers, 34 (1912), pp. 185–231.
[67] Wikipedia, *Redlich–kwong equation of state*, 2012. [Online; accessed 11-April-2012].
[68] P. J. Wong and R. E. Larson, *Optimization of natural-gas pipeline systems via dynamic programming*, IEEE Trans. Automat. Contr., 13 (1968), pp. 475–481.
[69] P. J. Wong and R. E. Larson, *Optimization of tree-structured natural-gas transmission networks*, J. Math. Anal. Appl., 24 (1968), pp. 613–626.

[70] S. Wright, M. Somani, and C. Ditzel, *Compressor station optimization*, in 30th Annual Meeting, Pipeline Simulation Interest Group, 1998. Paper 9805.
[71] S. Wu, *Steady-State Simulation and Fuel Cost Minimization of Gas Pipeline Networks*, ProQuest LLC, Ann Arbor, MI, 1998. Thesis (Ph.D.)-University of Houston.
[72] S. Wu, R. Z. Ríos-Mercado, A. E. Boyd, and L. R. Scott, *Model relaxations for the fuel cost minimization of steady-state gas pipeline networks*, Tech. Rep. TR-99-01, University of Chicago, January 1999.
[73] J. Záworka, *Project SIMONE—Achievements and running development*, in SIMONE [58], pp. 1–24.

Martin Schmidt, Marc C. Steinbach, Bernhard M. Willert, Leibniz Universität Hannover, Institute for Applied Mathematics, Welfengarten 1, 30167 Hannover, Germany
E-mail address: {mschmidt,steinbach,willert}@ifam.uni-hannover.de
URL: www.ifam.uni-hannover.de/~{mschmidt,steinbach,willert}